Light Metals 2015
Edited by: Margaret Hyland
TMS (The Minerals, Metals & Materials Society), 2015

ROLE OF SOLIDIFICATION CONDITIONS IN DETERMINING THE MICROSTRUCTURE OF Al-Si CAST ALLOYS

A.M. Samuel,[1] S.A. Alkahtani,[2] Kh. Abuhasel,[2] F.H. Samuel[1]

[1] Universite du Québec à Chicoutimi, QC, Canada
[2] Salman bin Abdulaziz University, Alkharj, Saudi Arabia

Keywords: Al-Si-Cu Alloys, Porosity, Hydrogen, Modification, Grain Refining, Statistical Analysis

Abstract

The influence of solidification conditions on the microstructure of Al-Si-Cu alloys was examined using two molds: an endchill mold that provided different cooling rates along the solidification axis, and a sand mold comprising different fins. Melt hydrogen, Sr, Ti levels were also varied. In all 24 alloys/135 conditions were investigated. Statistical analysis of porosity data for end-chill mold samples showed good fits for percentage porosity, and average/maximum pore area/pore length response parameters. At low solidification times, pores nucleated predominantly in intergranular regions, were mostly elongated, and occurred along the grain boundaries. Probability of pore nucleation in interdendritic regions increased at higher solidification times, and pores were more rounded. In sand castings, hydrogen levels of ~0.3 ml/100g produced extremely large pores, even at high cooling rates. For sound castings, proper melt degassing and preheating of the sand mold are essential to ensure against occurrence of reaction porosity along the casting surface.

Introduction

Cast aluminum alloys, particularly those belonging to the aluminum-silicon (Al-Si) system, have been developed over the years in keeping with the continuing demands of the aerospace and automotive industries for smaller, lighter-weight, and more cost-effective components possessing premium mechanical property and quality requirements [1-4].While developments in lightweight metals have traditionally been initiated by demands from the aerospace sector, the declining sales of the industry have turned the focus and market around to the commercial sector - primarily in the automotive field. In North America, the commercial potential of aluminum alloys has risen sharply, as evidenced by the increasing use of these materials in automobile components by companies like Ford, General Motors and Chrysler, as well as by European and Japanese carmakers [5]. Weight reduction - a prime consideration for all automakers, together with the metal's durability and its life cycle cost are the main factors that have encouraged these companies to increase the use of aluminum in their vehicles, and R & D efforts are continually being directed in furthering the development of improved Al-Si base alloys. The installation of an aluminum molding line at Metal Casting Operations for the production of cylinder heads amply witnesses this fact [6].

Two important factors that determine the eventual quality and properties of such cast components are the solidification rate and porosity: solidification rate affects the microstructure, as well as the porosity formed, whereas porosity affects the surface quality, soundness, corrosion resistance and other properties. Apart from solidification rate, microstructural control is also achieved through grain refinement and modification, where small additions of Al-Ti-B and Al-Sr master alloys, respectively, provide the means for producing refined microstructures and the required morphology of constituent phases [7].

As for porosity, its formation is attributed mainly to two effects: shrinkage, resulting from the volume decrease accompanying solidification, and the evolution of dissolved gases, resulting from the decrease in solubility of these gases in the solid as compared to the liquid metal. Hydrogen, the only gas capable of dissolving to a significant extent in molten aluminum but exhibiting very low solubility in the solid state, is mainly responsible for the gas porosity in a casting, together with the pressure during solidification, the chemical composition and solidification range of the alloy, and the solidification rate. Shrinkage porosity can also occur as "microshrinkage" or "microporosity", dispersed in the interstices of dendritic solidification regions. Limited or inadequate liquid metal feeding in the dendritic solidification area gives rise to this type of porosity [8-10].

Grain refining, modification and the inclusion content of the melt also influence porosity formation. Melt cleanliness, with particular regard to the presence of oxides and inclusions, is recognized as an important factor that influences hydrogen gas nucleation [11]. More often than not, the various factors contributing to porosity manifest themselves simultaneously, interacting with each other to develop the porosity observed.

Although porosity in aluminum alloys has been variously investigated, detailed systematic data on different alloy systems in terms of parametric studies of the porosity formation and distribution is generally not available. In particular, in the case of the cast aluminum alloy 319, which ranks as one of the commercially important alloys used in automotive applications on account of its excellent casting characteristics and good mechanical properties, relatively fewer studies are to be found in the literature compared to A356, another commercially important automotive alloy [12, 13]. In fact, studies reported by our group [14, 16] appear to be among the few that cover porosity formation in Al-Si-Cu-Mg alloys compared to the numerous investigations on Al-Si cast alloys.

This lack of design data, particularly in the know-how of controlling the formation of porosity and its effect on secondary properties (e.g., fatigue, wear, corrosion, etc.) in these alloys poses constraints on their applicability. Addressing this issue by providing such data would certainly remedy the situation. The

aim of the present project, therefore, was to distinguish the different factors affecting porosity and to determine their individual and combined effects on porosity formation in 319 alloys in relation to product quality; the systematic data generated from the work to be used to obtain a response surface model of the porosity behaviour of this alloy. The present investigation was undertaken to perform:
(a) A study of the effect of hydrogen content (0.1-0.4 ml/100g Al – 3 levels coded H1, H2, H3), modification (strontium: 0-300 ppm – 3 levels coded S1, S2, S3), and grain refinement (TiB_2: 0-0.02 wt%, coded T) on the porosity formation and distribution in 319 alloys (24 alloys representing H, HS, HT and HTS series).
(b) A parametric study of the evolution of porosity in the Al-Si-Cu-Mg system in order to develop a response surface model of the porosity behaviour of this alloy system as a function of alloy and process parameters.

Experimental Procedures

The 319.2 aluminum alloy used in this study was supplied in the form of 12.5-kg ingots. The chemical composition of the as-received alloy is shown in Table 1. The ingots were melted in a silicon carbide crucible of 7 kg capacity, using an electric resistance furnace. The melting temperature was held at 735 ± 5°C. At this temperature, the molten metal was either degassed using high purity argon or gassed (H_2~0.32-0.36 ml/100g Al). Melts were also modified using Al-10wt%Sr master alloy (~70-90 ppm Sr level) and grain refined by means of Al-5wt% Ti-1wt%B master alloy to obtain a 0.02 wt% Ti content.

Casting was done using a rectangular-shaped end chill mold made of refractory material. The chill consisted of a copper box at the bottom through which cold water was circulated. Prior to casting, the mold was preheated to 150°C to drive out moisture. Table 2 indicates the average dendrite arm spacings (DASs) and local solidification times that were obtained from their cooling curves corresponding to different distances from the chill end.

Samples were sectioned from the cast blocks in the horizontal orientation at varying heights (5, 10, 20, 40 and 100 mm) above the water-chilled copper base, from which metallographic or tensile test sheet specimens were prepared for metallographic observations or tensile testing purposes [10], respectively.

For the sand mold castings, alloy melts were poured into the cooling fin sand molds preheated to about 105°C to remove moisture. Preliminary investigations of the microstructures obtained from the different fin sections gave dendrite arm spacings (DASs) as shown in Table 3. From these it was decided to select the fins #s 1, 5 and 9 for comparison purposes with end-chill samples having similar DASs.

Results and Discussion

A-End Chill Mold Cast Microstructures

Before sectioning the end-chill castings for preparing the metallographic and tensile test specimens, they were radiographically examined to obtain an idea of the general pore morphology and distribution in the three H1 (0.1ml/100g), H2 (0.25ml/100g) and H3 (0.36ml/100g) alloy series. The main observations noted from the corresponding radiographs were as follows.
(i) For a given hydrogen content, pore density increased with increase in local solidification time, i.e., proceeding from the end-chill bottom to the top of the casting.
(ii) Increasing the hydrogen level intensified the pore density with a marked decrease in the central sump shrinkage cavity.
(iii) Addition of strontium (i.e. HS3 ingots) contributed significantly to the increase in pore density.
(iv) Grain refiner addition (in terms of a 0.02 wt% Ti addition) decreased the grain size, leading to finer pore sizes compared to the H ingots. However, it did not have an influence in increasing the pore density, as HTS3 ingots showed lower pore densities than HS3 ingots, probably due to the fact that the original TiB_2 particles in the as-received alloy lost their grain refining effect (termed "fading") during remelting of the alloy.

Porosity measurements were carried out for all castings produced. Parameters measured were the average and maximum pore area, pore length and the percentage porosity. Overall observations were summarized as follows.
1. Variation in dendrite arm spacing (DAS) and grain size as a function of local solidification time is shown in Figure 1. The addition of TiB_2 (H1T alloy) leads to a significant reduction in the grain size, and also a reduction in the DAS compared to the base alloy H1. The increase in DAS and grain size is observed to be relatively slow for distances >40 mm from the chill end.
2. The changes in the average Si particle area and length obtained for the alloy for different strontium additions to the melt are shown in Figure 2. It can be seen that the Si particle size is dependent on the α-Al DAS. Apparently, for the low Si content of the alloy (~6 wt%), an addition of 90 ppm Sr is sufficient to produce more or less complete modification of the Si particles, even at cooling rates of 0.4°C/s (DAS ~90 μm).
3. Among the intermetallics and other constituents observed in the microstructure, the ß-iron Al_5FeSi phase (observed in the form of needles in the microstructure) is known for its detrimental influence on the tensile properties. The brittle nature of the ß-needles and their sharp tips create zones of localized stress that contribute to the degradation in properties [10].

Our earlier studies [3, 11] have shown that these ß-needles are very active as pore nucleation sites in that small pores are often found nucleated along the long sides of the needles. Such a mechanism is expected to result in an increase in pore density, which is strongly related to the metal feedability or the ease with which the molten metal can flow into the different sections of the casting mold. However, in spite of the harmful effect of the ß-needles as pore nucleation sites, their presence seems to limit pore growth. Figure 3 shows how the ß-needles limit the lateral growth of both gas and shrinkage pores. Proper control of this phase thus becomes important from both properties and porosity points of view. Essential features observed in regard to the occurrence of the ß-Al_5FeSi phase in this study are as follows.

(i) The DAS critically affects the size of the ß-needles, the latter being indicative of the volume fraction of the phase obtained in the sample. Figure 4 shows the microstructures of H1 alloy sample (degassed alloy, no melt treatment) obtained from the 100mm level above the chill, revealing an abundant number of β-platelets at this slow cooling rate.
(ii) In the unmodified alloy (H1), sympathetic (preferential) nucleation of the needles is observed, leading to the branching of several needles from a parent needle. Addition of Sr is seen to reduce this effect, the Sr poisoning the nucleation sites and assisting in the dissolution of the ß-needles. An addition of 300 ppm Sr (H1S3 alloy) is seen to accelerate the dissolution process, leading to the fragmentation of the needles into smaller segments (*cf.* 60-80μm with 120-1200μm in untreated H1 alloy).

Table I Chemical composition of the 319.2 alloy (wt%).

Element (wt%)								
Si	Cu	Fe	Mn	Mg	Ti	Sr	Zn	Ni
6.23	3.77	0.46	0.14	0.06	0.073	0.0003	0.08	0.008

Table II Variation in local solidification time and dendrite arm spacing as a function of distance from the chill end.

Distance from chill end (mm)	Local solidification time(s)	Average DAS (μm)
5	172	15
10	222	28
20	345	52
40	593	73
100	1222	95

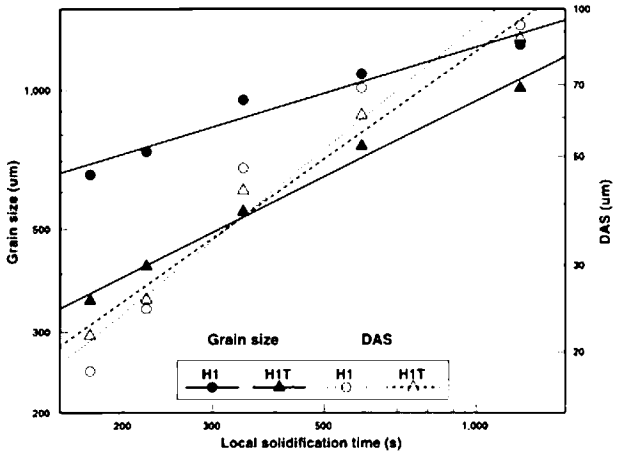

Figure 1. Variation in grain size and DAS as function of local solidification time for H1 and H1T alloys.

Figure 3. Role of ß-Al_5FeSi needles in restricting the growth of a gas pore. Note the presence of small pores along the long sides of the ß-needles (arrowed).

(iii) A tendency for thickening of the ß-needles is observed with grain refining, along with the sympathetic nucleation/branching effect noted in the untreated alloy. The thickening takes place via a step-like motion of ledges as shown in Figure 5. Brittle fracture of thick needles was observed to occur, different from the fragmentation that occurs due to Sr modification.
(iv) A comparison of the ß-needle densities for H1, H1T, H1S3 and H1TS3 alloys at the 100 mm level (DAS ~90 μm) reveals that the H1S3 alloy sample gives the lowest needle density

Table III. Variation in dendrite arm spacing as a function of fin thickness in cooling fin sand mold casting.

Fin No.	Fin thickness (mm)	Average DAS (μm)
1	2.5	25
5	7.5	53
9	24.5	85

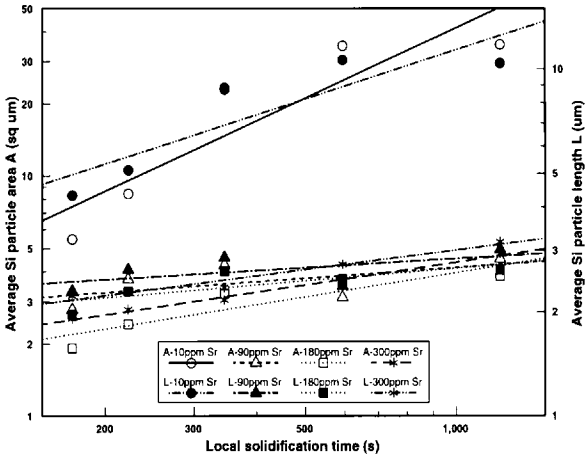

Figure 2. Variation in average Si particle area A (μm^2) and length L (μm) as a function of local solidification time for different Sr concentrations.

Figure 4. Microstructure of H1 alloy sample obtained at 100mm level above the chill end showing the relative abundance of ß-Al_5FeSi needles.

(Figure 6). Addition of grain refiner decreases the beneficial effect obtained with Sr addition.

Figure 7 presents the microstructure of H1 alloy. At 100mm distance from the chill, pores were seen in the interdendritic regions, disconnected, their lengths approximately the same as the dendrite arms or even less. The microstructure of H1S3 alloy at 100mm is shown in Figure 8. The pores were rounded, and an increase in both pore size and percentage porosity was observed.

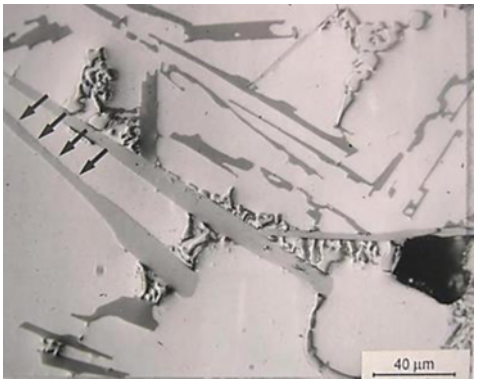

Figure 5. Microstructure of H1T alloy at 100 mm distance above the chill, showing (a) thickening of the ß-Al5FeSi needle via a step-like motion of ledges (arrowed).

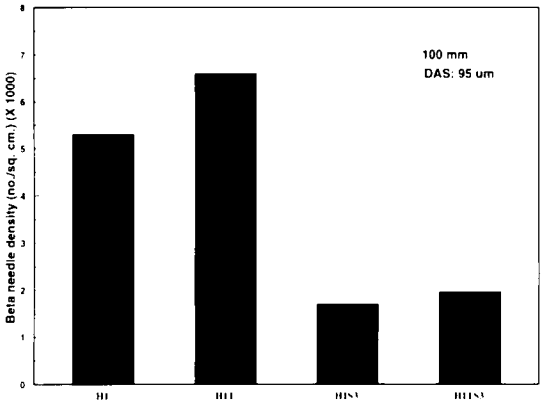

Figure 6. Histogram comparing the ß-needle densities of H1alloys at 100 mm distance from the chill end.

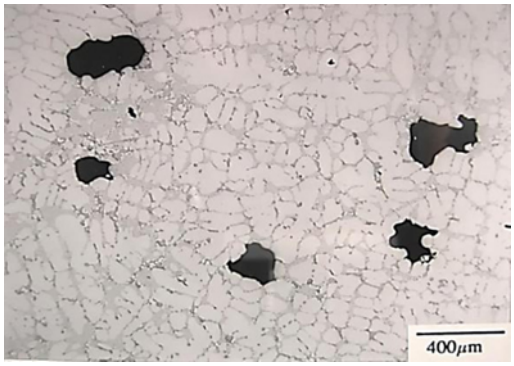

Figure 7. Microstructures showing porosity distribution in H1 alloy at 100mm distance above the chill end.

In the grain refined alloy (H1T), a well dispersed distribution of small pores was observed, the pores occurring either at the grain boundaries or within the grains. The variation in percentage porosity with DAS for degassed and filtered melt castings of the H1 alloys under different melt treatment conditions is summarized in Figure 9.

It is well established that hydrogen is the strongest determinant of all the parameters that contribute to porosity formation. This was clearly evidenced from the microstructures of the H3 alloy samples. At 5mm distance from the chill, two distinct pore morphologies, elongated and rounded, could be observed, as

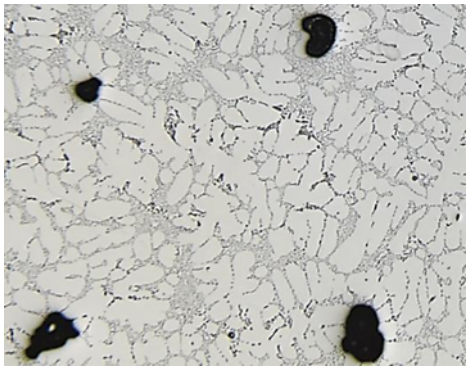

Figure 8. Microstructures showing porosity distribution in H1S3 alloy at 100mm distance above the chill end.

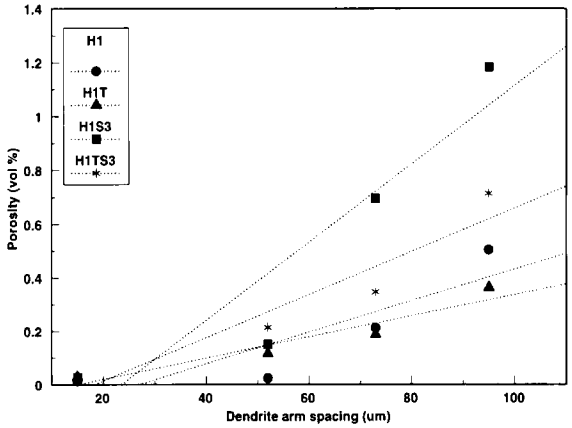

Figure 9. Variation in % porosity with DAS for H1 alloys.

shown in Figure 10(a). At 100mm distance, however, the majority of pores were rounded, Figure 10(b). The hydrogen-strontium interaction effect on porosity (H3S3 alloy containing 300ppm Sr) resulted in pores that were mostly round as opposed to the mixture of rounded and elongated forms observed in the case of H3 alloy (at 5mm distance from the chill). This treatment was also associated with an increase in the areal pore density. An increase in the solidification time (i.e., at 100 mm above the chill) resulted in pores that were larger and more spherical than those observed in H3 alloy.

Samples obtained from H3TS3 alloy (containing 0.02%Ti) and etched in Keller's reagent were examined to determine the nucleation mechanism of pores. At low solidification times (5 mm distance from the chill) the pores (elongated or rounded) were mostly found nucleated at or along the grain boundaries. At intermediate solidification times (20 mm distance from the chill), while most of the pores were nucleated in the intergranular regions, some were observed in the interdendritic regions, Figure 11. At the highest solidification time (100 mm distance from the chill) also, the possibility of pore nucleation in the intergranular regions was still evident.

As mentioned previously, the porosity data for the 135 end-chill, and 24 sand-cast samples was further analysed to obtain (i) pore density vs. pore area and (ii) pore density vs. pore length distributions, from which the average and maximum pore area/pore length values and respective pore densities were determined for the two parts of the distribution curves representing small and large pores. The area percent porosity was also determined in each case. These values constitute the

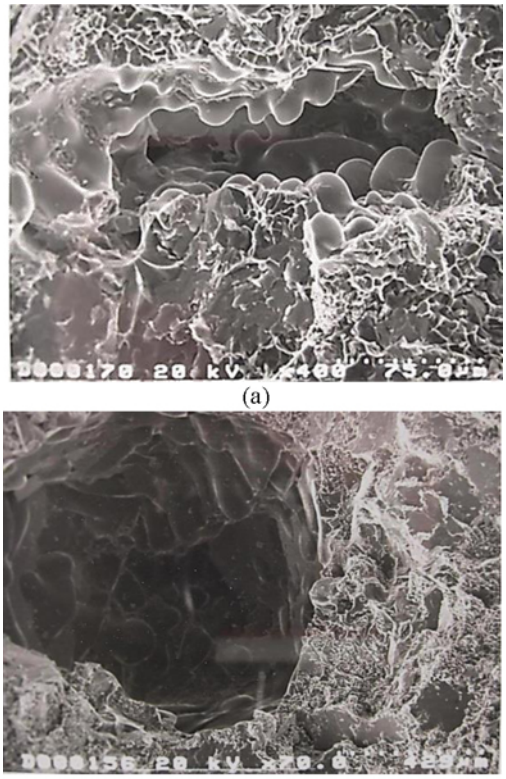

(a)

(b)

Figure 10. Microstructures of H3 alloy samples at (a) 5mm, and (b) 100mm distance from the chill end.

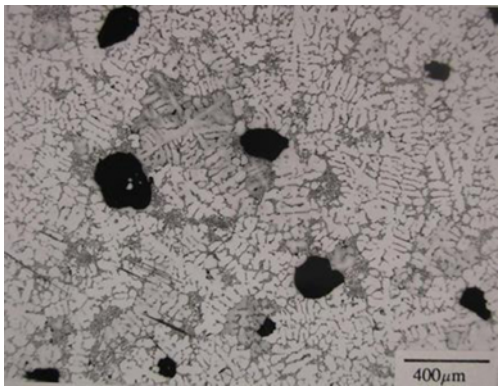

Figure 11. Microstructure obtained from H3TS3 alloy sample, etched in Keller's reagent.

response parameters that are obtained as a result of the alloy parameters (chemical composition) and thermal parameters (solidification time and solidus velocity) of each sample (viz., the predictor or controlling parameters).

B-Sand Mold Cast Microstructures

The porosity data obtained from image analysis for the sand cast samples was treated as described previously, to obtain the average and maximum pore area/pore length values, and respective pore densities for the two parts of the corresponding pore density vs. pore area and pore density vs. pore length distribution curves, pertaining to the small and large pores. The area percent porosity was also determined in each case. The sand cast fin samples exhibited essentially the same microstructural features as those of the endchill cast samples. As shown in Table 3, the dendrite arm spacing (DAS) increased from 25 μm to 85 μm on proceeding from fin #1 to fin #9. The size of the microstructural constituents also varied, accordingly.

From the porosity point of view, the H1 samples, particularly fin #s 1 and 5, were seen to exhibit tiny pores scattered randomly over the sample surface. The fin #5 sample of H1 alloy clearly revealed that the porosity was mainly shrinkage-type. Increasing the hydrogen level to H3 produced a dramatic change in the amount of porosity observed in the fin samples (Figure 12). The rounded morphology of these pores in Figure 13 is typically characteristic of gas porosity. With grain refiner addition, the pore morphology tended to be predominantly spherical, as shown in Figure 14 (a) for H3T alloy samples corresponding to fin # 5.Strontium addition, on the other hand, produced irregular pore morphology, as observed in the case of the H3S3 fin #1 sample shown in Figure 14(b).

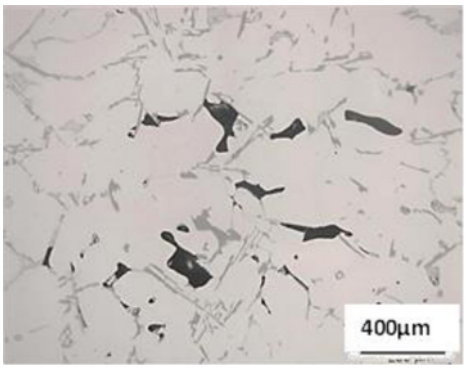

Figure 12. Microstructure showing porosity distribution in sand cast sample of H1 alloy fin #9, showing shrinkage-type porosity.

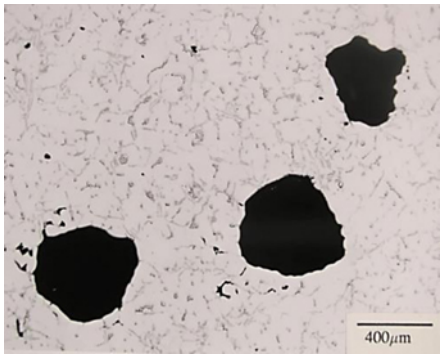

Figure 13. Microstructure showing porosity distribution in sand cast sample of H3 alloy fin #5, showing gas-type porosity.

Thus, for producing sound sand castings, it is important that the melt hydrogen level should not exceed 0.1 ml/100 g, i.e., the melt should be properly degassed, as at high hydrogen levels, even the influence of a high cooling rate is not sufficient to prevent the occurrence of large pores in the solidified structure. Also, proper preheating of the sand mold before casting will ensure against the occurrence of reaction porosity along the casting surface.

C-Statistical Analysis of Porosity Distribution using Multiple Regression

Statistical analysis using data reduction techniques has been increasingly applied to quantitatively predict porosity formation in alloy castings based on the results obtained from a planned set

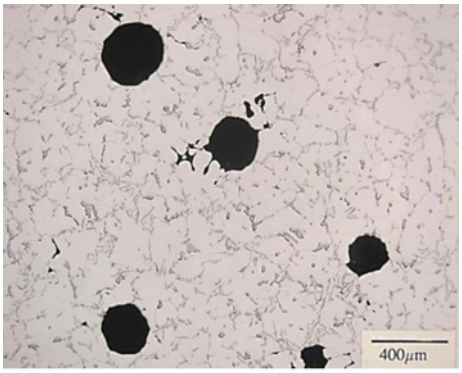

(a)

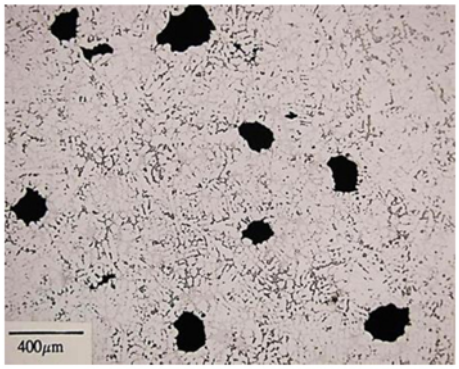

(b)

Figure 14. Microstructures of sand cast alloy samples showing the effect of: (a) grain refiner addition in H3T alloy-fin #5 sample, and (b) combined influence of Sr and grain refiner additions in H3TS3 alloy-fin #5 sample.

of experiments (factorial design), where the response parameters (porosity) can be quantitatively related to the predictor parameters (alloying and melt conditions). This methodology is very efficient in that it not only provides information with much less effort, but also provides information about the interactions between the controlling variables, which is a significant factor in the search for optimum conditions – in this case that of obtaining quality castings with minimum porosity. This approach, termed Response Surface Methodology has been successfully applied to other Al alloy systems [7, 18].

In the present case, the method of multiple regression analysis using stepwise reduction was selected, due to its ability to detect and evaluate the interactive effects of the predictor parameters on the response parameters [19, 20]. The analysis was carried out using the Statistica for Windows software program supplied by StatSoft Inc. [21]. Data sets for the endchill and sand mold samples were built up using both independent and dependent variables. The thirteen independent or controlling parameters were the alloy parameters, i.e., Si, Cu, Zn, Fe, Mg, Mn, Ti compositions, as well as the Sr and hydrogen levels, the grain refiner addition, the DAS and the solidification time (TS) and solidus velocity (VS). Predictor terms were constructed using these variables and tested for their ability to predict the response (porosity) parameters. The two data sets were explored using the Statistica software program, to find the predictor terms that gave the best possible fit to the data set. This was done by evaluating the R^2 value (fraction of variance of the data set, with $R^2 = 1$ representing a perfect correlation), the t-value (to assess the relative strength of each predictor term), and the p-level or significance number (measure of the relative significance of each term), where the closer to zero the p-level, the more certain the relationship between the predictor term and the response parameter.

Table IV summarizes the predictor variables used to develop the various response surface models (response parameters), and the t-values and significance levels obtained for each predictor in the respective cases. As may be noted, hydrogen is the parameter that has the greatest impact on the percentage porosity, followed by the DAS, and then Sr, these parameters showing the highest t-values and zero significance levels (the 0.00000 p-levels quoted in the table are actually 0.000000). However, as far as the other response parameters are concerned, i.e., those that correspond to the pore size (pore area/pore length), it is the DAS that has the greater influence compared to hydrogen. The strongest impact of DAS is on the maximum pore area, with a t-value of 22.35 compared to 8.721 for hydrogen.

In the case of the end-chilled samples, good fits were obtained for almost all the response parameters, viz., for percentage porosity, and maximum pore area, average pore area, maximum pore length, and average pore length for the irregular part of the porosity distribution curves (i.e., big pores), with R2 values ranging between 0.873 and 0.768. The maximum pore area showed the highest R2 value (0.873), with percentage porosity (0.832) and average pore area (0.831) following closely. For all models, the predictor variables were H, DAS, Sr, Ti and Mg, with solidification time (TS) and Cu as additional predictors in some of the models, like those for percentage porosity and average pore area.

Comparing the effects of Sr and Ti additions, Sr has the greater influence on the percentage porosity and average and maximum pore area parameters. Pore lengths, on the other hand, are controlled more by Ti than by Sr. This is to be expected, in view of the effect that grain refiner addition has on reducing the grain size and, hence, the grain boundary facets along which the pores form, in other words, the pore lengths. These results support the qualitative microstructural observations of porosity distribution.

With respect to the sand cast samples, a good fit was obtained solely for percentage porosity (with an R2 value of 0.859). None of the other response parameters could be fitted with the data available. The reason for this is mainly attributed to the limited experimental data available (24 cases only), as well as the extremely large pore areas observed in the case of these samples, in particular, those corresponding to the H3 alloys. Another possibility could be the difference in the mode of solidification for the two mold types, where the two thermal parameters of solidification time and solidus velocity that satisfactorily account for the mold factor in the end-chill mold samples may not be adequate in the sand mold case. In their study of microporosity formation in A356 alloy, Tynelius et al. [7] have also reported that much larger pore sizes are obtained for sand castings compared to permanent mold castings.

As in the percentage porosity model for the end-chill samples, the predictor variable having the strongest impact on the percentage porosity for the sand cast samples was hydrogen, followed by the DAS, as seen in Table IV. The influence of the DAS was somewhat reduced compared to the end-chill case. Colored 3D contour plots of various response parameters were plotted as a function of two predictor variables at a time for the end-chill and sand mold cases. Figure 15 (a-c) shows the 3D surface plots obtained from the endchill mold under different working conditions. For a given hydrogen level, decreasing the

cooling rate (Figure 15(a)) leads to remarkable increase in the percentage porosity. Addition of Sr up to 350ppm also contributes to porosity formation but to a lesser extent compared to that obtained from cooling rate (Figure 15(b)). Grain refining using TiB_2 is the only parameter that is seen to reduce the percentage porosity (Figure 15(c)).

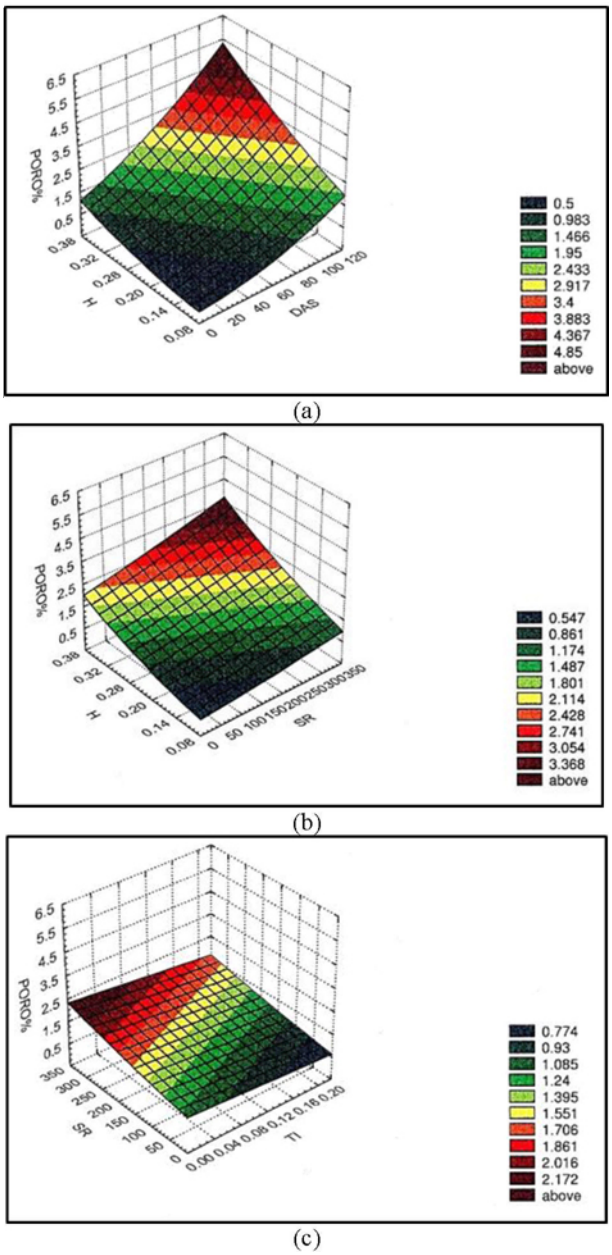

Figure 15. The 3D response surface plots obtained for endchill mold cast samples showing variation in percentage porosity as a function of (a) H_2-DAS, (b) H_2-Sr, and (b) Sr-Ti interactions.

Figure 16 (a, b) presents the 3D surface plots produced from the cooling fin sand mold revealing similar behaviour or trend of cooling rate (fin thickness) and grain refiner as that exhibited by the samples obtained from the end chill mold.

Conclusions

1. With respect to solidification time (as a function of DAS), the interaction effect of other parameters, namely hydrogen (H_2),

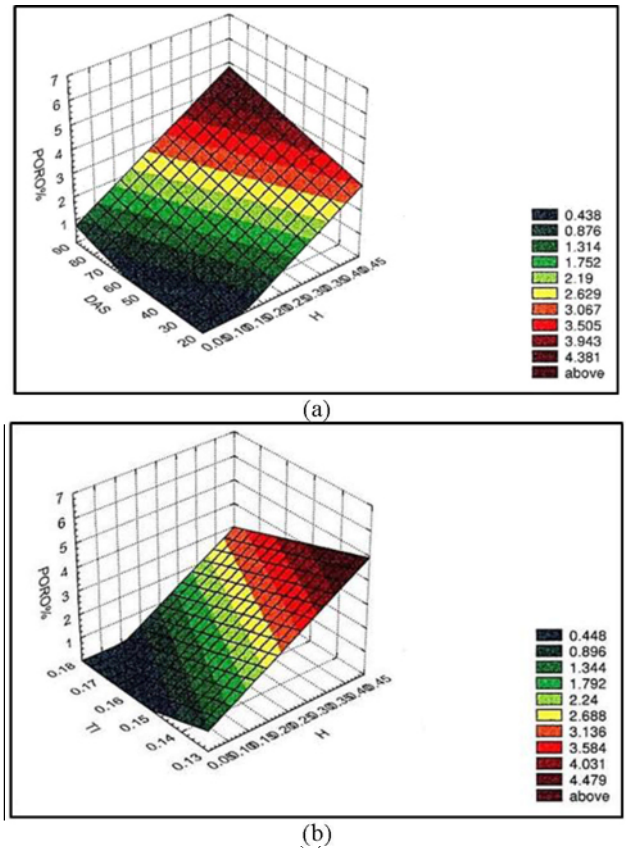

Figure 16. The 3D response surface plots for percentage porosity obtained from sand mold cast samples as a function of (a) DAS-H_2, and (b) grain refiner-H_2 interactions.

modifier (Sr) and grain refiner (TiB_2) levels on porosity follows the order: H_2 > Sr > TiB_2 .

2. At low solidification times, pore nucleation takes place predominantly in intergranular regions, pores are mostly elongated and lie along the grain boundaries. Probability for pore nucleation in interdendritic regions increases at higher solidification times, and the pores tend to be more rounded.

3. Addition of Sr enhances the sphericity of the pores and increases the porosity vol% and pore size. Grain refining results in smaller pores, well dispersed within the casting. Sr improves alloy ductility and also poisons nucleation sites of ß-Al_5FeSi phase needles Fragmentation and dissolution of ß-needles takes place with increasing Sr, reducing their harmful effect.

4. H_2 levels of ~0.3 ml/100g produce extremely large pores in sand castings, even at high cooling rates. To produce sound castings, the melt be properly degassed to minimize the H_2 level.

5. For endchill mold samples, good fits for %porosity, max pore area, av pore area, max pore length, and av pore length are obtained from statistical analysis of the porosity data, validating microstructural/qualitative observations reported previously [3]. Hydrogen has the greatest influence on %porosity, followed by DAS and Sr. Pore size is controlled more strongly by DAS than by H_2, the strongest impact of DAS being on the max pore area. Whereas % porosity and pore area are more influenced by Sr than by Ti addition, pore length is controlled to a greater extent by the latter. Magnesium is also observed to have an influence comparable to that of hydrogen on the pore size (area/length).

6. For sand-cast samples, due to the limited experimental data available, a good fit of the statistical data is obtained only for the percentage porosity, where, as in the end-chill case, hydrogen is seen to have the strongest impact, followed by the DAS.

Acknowledgements
The authors would like to thank Ms. Amal Samuel for enhancing the art work and Mr. G. Zaki for assisting in the preparation of the manuscript.

References

1. R.J. Garino and S. Wakesberg, "Automobile material choices," Scrap Processing & Recycling, 51(5) (Sept-Oct, 1994), 101-105.
2. Z. Ma, "Effect of Fe-Intermetallics and Porosity on Tensile and Impact Properties of Al-Si-Cu and Al-Si-Mg Cast Alloys", Ph.D. Thesis, Université du Québec à Chicoutimi, Canada, Nov., 2003.
3. A.M. Samuel, F.H. Samuel, and H.W Doty, "Observations on the Formation of β-Al5FeSi Phase in 319 type Al-Si Alloys," Journal of Materials Science, 31 (20) (1996), 5529-5539.
4. J. Espinoza-Cuadra et al., "Effect of Sr and Solidification Conditions on Characteristics of Intermetallic in Al-Si 319 Industrial Alloys," Materials and Design, 31(1) (2010), 343-356.
5. L. Li et al., "Role of iron in relation to silicon modification in Sr-treated 319 and 356 alloys," International Journal of Cast Metals Research, 16 (4) (2003), 397-408.
6. L. Li et al., "Characteristics of alpha-dendritic and eutectic structures in Sr-treated Al-Si casting alloys. Journal of Materials Science, 39 (1) (2004), 215-224.
7. K. Tylenius, J.F. Major, and D. Apelian, "Optimization of Casting Parameters for Production of Sound Al Castings: A Response Surface Methodology Approach," AFS Transactions, 101 (1993), 401-413.
8. H.R. Ammar, A.M. Samuel, and F.H. Samuel, "Effects of surface porosity on the fatigue strength of AE425 and PM390 hypereutectic Al-Si casting alloys at medium and elevated temperatures," Mater. Sci. Eng. A, 473 (1-2), (2008), 58-64.
9. G.A. Edwards et al., "Microporosity Formation in Al-Si-Cu-Mg Casting Alloys," AFS Transactions, 105 (1997), 809-818.
10. A. M. Samuel and F. H. Samuel, "A metallographic study of porosity and fracture behavior in relation to the tensile properties in 319.2 end chill castings," Metallurgical and Materials Transactions A, 26 (1995), 2359-2372.
11. N. Roy, A.M. Samuel, and F.H. Samuel, "Porosity formation in AI-9 Wt pct Si-3 Wt pct Cu alloy systems: Metallographic observations," Metall. Mater. Trans. A, 27A (1996), 415-429.
12. C. Dupuis, Z. Wang, J-P. Martin, and C. Allard, in E.R. Cutshall, ed., Light Metals 1992 (Warrendale, PA: The Minerals, Metals and Materials Society, 1992), 1055-1068.
13. H.R. Ammar, A.M. Samuel, and F.H. Samuel, "Porosity and the fatigue behavior of hypoeutectic and hypereutectic aluminum-silicon casting alloys," International Journal of Fatigue, 30 (6) (2008), 1024-1035.
14. L. Liu et al., "Precipitation of β-Al_5FeSi phase platelets in Al-Si based casting alloys," Metallurgical and Materials Transactions A, 40 (10) (2009), 2457-2469.
15. Z. Ma et al., "A study of tensile properties in Al-Si-Cu and Al-Si-Mg alloys: Effect of β-iron intermetallics and porosity," Materials Science and Engineering A, 490 (1-2) (2008), 36-51.
16. Z. Ma et al., "Parameters controlling the microstructure of Al-11Si-2.5Cu-Mg alloys," Materials & Design, 31 (2) (2010), 902-912.
17. N. Roy, M. Eng. Thesis, UQAC, Chicoutimi, Canada (1995).
18. N. Roy, P.R. Louchez, and F.H. Samuel, "Statistical analysis of porosity in Al-9 wt % Si-3 wt % Cu-X alloy systems," Journal of Materials Science, 31 (1996), 4725-4740.
19. G.E.P. Box, W.G. Hunter, and J.S. Hunter, Statistics for Experimenters (New York: John Wiley & Sons, Inc., 1978).
20. Leslie Davies, Efficiency in Research, Development and Production: The Statistical Design and Analysis of Chemical Experiments (Cambridge, U.K.: The Royal Society of Chemistry, 1993).
21. STATISTICA release 5 (Quick Reference) Manual and brochure, StatSoft, Inc., Tulsa, OK 74104 (1995).

Table IV Response surface models obtained for porosity behavior in end-chill and sand-cast samples

Response Parameter (Model)	Predictor Variables Used in Model (T-values and significance levels given below each)							R^2 value
End Chill Mold								
Percentage Porosity	**H**	**DAS**	**Sr**	**Ti**	**Mg**	**Cu**	**TS**	0.832
	9.470	7.902	6.564	-2.910	3.674	3.112	-2.078	
	.00000	.00000	.00000	.00426	.00035	.00228	.03969	
Maximum Pore Area (μm^2)	**H**	**DAS**	**Sr**	**Ti**	**Mg**			0.873
	8.721	22.350	4.782	-3.684	8.403			
	.00000	.00000	.000005	.00033	.00000			
Average Pore Area (μm^2)	**H**	**DAS**	**Sr**	**Ti**	**Mg**	**Cu**	**TS**	0.831
	6.125	11.085	7.0599	-3.838	5.316	2.494	-2.821	
	.00000	.00000	.00000	.00019	.00000	.01388	.00555	
Maximum Pore Length (μm)	**H**	**DAS**	**Sr**	**Ti**	**Mg**		**TS**	0.812
	6.061	7.110	4.682	-5.458	6.346		3.376	
	.00000	.00000	.000007	.00000	.00000		.00097	
Average Pore Length (μm)	**H**	**DAS**	**Sr**	**Ti**	**Mg**			0.768
	5.333	16.639	3.478	-5.145	5.167			
	.00000	.00000	.000687	.000001	.000001			
Sand Mold								
Percentage Porosity	**H**	**DAS**	**Int VS-Ti**	**Ti**				0.859
	9.212	3.754	2.137	-2.863				
	.00000	.00145	.04655	.01033				